

Non-linear evolution and parton distributions at LHC and THERA energies

M. Lublinsky,^{* a)} E. Gotsman,^{† b)} E. Levin,^{‡ b)} and U. Maor,^{§ b)}

*a) Department of Physics
Technion – Israel Institute of Technology
Haifa 32000, ISRAEL*

*b) HEP Department
School of Physics and Astronomy
Raymond and Beverly Sackler Faculty of Exact Science
Tel Aviv University, Tel Aviv, 69978, ISRAEL*

October 27, 2018

Abstract

We suggest a new procedure for extrapolating the parton distributions from HERA energies to higher energies at THERA and LHC. The procedure suggested consists of two steps: first, we solve the non-linear evolution equation which includes the higher twists contributions, however this equation is deficient due to the low ($\log(1/x)$) accuracy of our calculations. Second, we introduce a correcting function for which we write a DGLAP type linear evolution equation. We show that this correcting function is small in the whole kinematic region and decreases at low x . The nonlinear evolution equation is solved numerically and first estimates for the saturation scale, as well as for the value of the gluon density at THERA and LHC energies are made. We show that non-linear effects lead to damping of the gluon density by a factor of $2 \div 3$ at $x \approx 10^{-7}$.

*e-mail: mal@techunix.technion.ac.il

†e-mail: gotsman@post.tau.ac.il

‡e-mail: leving@post.tau.ac.il

§e-mail: maor@post.tau.ac.il

1 Introduction

The standard perturbative QCD approach to deep inelastic scattering processes is based on two main ideas:

- the DGLAP evolution equations [1] for the leading twist parton distributions;
- the belief that if we start QCD evolution from sufficiently high $Q^2 \approx 2 - 4 \text{ GeV}^2$ the higher twist contributions are small.

The DGLAP evolution has two principal difficulties. First, the evolution predicts a steep growth of parton distributions in the region of low x which contradicts the unitarity constraints [2]. Hence, we can expect large corrections to the DGLAP evolution equation, at least in the region of low x . The second problem is of a general nature for perturbative QCD. It is well known that any perturbative series is an asymptotic one. Therefore, the correct estimates for the errors in the pQCD approach is the value of the next order term. Practically, this means that if we calculated the leading order gluon density distribution, say xG^{LO} , and the next to leading order one xG^{NLO} , then the correct estimates for the errors will be $\Delta xG = xG^{NLO} - xG^{LO}$, provided that the very same initial conditions are used. Such errors are large, especially at low x^1 .

It has been shown over the last two decades, that the generally held view on higher twist contributions is not correct [3]. Taking into account only two terms in Operator Product Expansion for a parton distribution (xG) we have

$$xG(x, Q^2) = xG^{LT}(x, Q^2) + \frac{M^2}{Q^2} xG^{HT}(x, Q^2) + O\left(\frac{M^4}{Q^4}\right),$$

with the high twist term $xG^{HT}(x, Q^2) \propto \left(xG^{LT}(x, Q^2)\right)^2$ in the region of low x [3]. The leading twist function $xG^{LT}(x, Q^2)$ sharply increases at $x \rightarrow 0$. Hence, we cannot conclude that the higher twist contributions are small in the whole kinematic region even if they are small for the initial value of $Q^2 = Q_0^2$. The scale M is introduced for dimensional reasons.

In this paper, we suggest a remedy for these two difficulties. First, we propose solving a nonlinear evolution equation which takes into account the most significant higher twist contributions and which specifies a high energy (low x) behavior of the parton densities, which are in accordance with the unitarity constraints. The parton distributions which we obtain are then amended by adding to the solution of the nonlinear equation \tilde{N} , a correcting function ΔN such that $N = \tilde{N} + \Delta N$. We then write a linear DGLAP-type equation for ΔN . Since ΔN in our approach vanishes at low x we expect this function to be small and concentrated in the region of moderate x . Consequently, this function should be free from all difficulties inherent in the usual scheme solutions of the DGLAP equation. We would like to mention here that our approach is very close to that of Kimber, Kwiecinski and Martin [4]. However, our treatment differs in the practical way that the programme is realized.

¹The widely held opinion that the NLO parton distributions describe the experimental data better is based on the fact that we can change the initial parton distribution drastically and achieve a better description.

An extrapolation of the available parton distribution to the region of lower x is a practical problem for LHC energies. We need to know the parton distribution both for estimates of the background of all interesting processes at the LHC, such as Higgs production, and for the calculation of the cross sections of the rare processes which the LHC is likely to measure. In this paper we will show that non-linear evolution will provide a considerable taming of the parton distribution in the LHC range of energies, by a factor of two - three in comparison with predictions based on the DGLAP linear evolution. We show here that the non-linear evolution considerably diminishes the value of the gluon density at $x = 10^{-5} \div 10^{-6}$ which is the energy range of the THERA electron - proton collider [5]. Therefore, our calculations provide the first estimates for the possible collective effects of high parton density QCD at THERA based on the correct non-linear evolution equation.

The paper is organized as follows. In the next section we formulate our approach and write a nonlinear equation for \tilde{N} and linear equation for ΔN . Section 3 is devoted to a numerical solution of the nonlinear equation. The following Section 4 presents some estimates of the corrections induced by the DGLAP kernel. The linear BFKL equation is discussed in Section 5. In the Section 6 we summarize our results and mention our plans for the future.

2 A new approach to DIS

The DGLAP equation describes the gluon radiation which leads to an increase in the number of partons. However, when the parton density becomes large, annihilation processes become active and they suppress the gluon radiation and, so, they tame the rapid increase of the parton densities at a new saturation scale $Q_s(x)$ [2, 6, 7]. The theoretical approach as well as understanding the physics of parton saturation is one of the most challenging problem of QCD which has stimulated the development of new methods [2, 6, 7, 8, 9, 10, 11, 12], surprisingly, all approaches lead to the same nonlinear evolution equation.

$$\begin{aligned} \tilde{N}(\mathbf{x}_{01}, Y; b) &= \tilde{N}(\mathbf{x}_{01}, Y_0; b) \exp \left[-\frac{2 C_F \alpha_S}{\pi} \ln \left(\frac{\mathbf{x}_{01}^2}{\rho^2} \right) (Y - Y_0) \right] + \\ &\quad \frac{C_F \alpha_S}{\pi^2} \int_{Y_0}^Y dy \exp \left[-\frac{2 C_F \alpha_S}{\pi} \ln \left(\frac{\mathbf{x}_{01}^2}{\rho^2} \right) (Y - y) \right] \times \\ &\quad \int_{\rho} d^2 \mathbf{x}_2 \frac{\mathbf{x}_{01}^2}{\mathbf{x}_{02}^2 \mathbf{x}_{12}^2} \left(2 \tilde{N}(\mathbf{x}_{02}, y; \mathbf{b} - \frac{1}{2} \mathbf{x}_{12}) - \tilde{N}(\mathbf{x}_{02}, y; \mathbf{b} - \frac{1}{2} \mathbf{x}_{12}) \tilde{N}(\mathbf{x}_{12}, y; \mathbf{b} - \frac{1}{2} \mathbf{x}_{02}) \right) \end{aligned} \quad (2.1)$$

The equation is written for $N(r_{\perp}, x; b) = \text{Im} a_{dipole}^{el}(r_{\perp}, x; b)$ where a_{dipole}^{el} is the amplitude for elastic scattering for a dipole of size r_{\perp} . The total dipole cross section is given by

$$\sigma_{dipole}(r_{\perp}, x) = 2 \int d^2 b N(r_{\perp}, x; b). \quad (2.2)$$

The deep inelastic structure function F_2 is related to the dipole cross section

$$F_2(x, Q^2) = \frac{Q^2}{4\pi} \int d^2 r_{\perp} \int dz |\Psi^{\gamma^*}(Q^2; r_{\perp}, z)|^2 \sigma_{dipole}(r_{\perp}, x), \quad (2.3)$$

where the QED wave functions Ψ^{γ^*} of the virtual photon are well known [13, 14, 15]. The meaning of Eq. (2.3) is simple since it describes the two stages of DIS[16]. The first stage is the decay of a virtual photon into a colorless dipole ($q\bar{q}$ -pair) which is described by wave function Ψ^{γ^*} in Eq. (2.3). The second stage is the interaction of the dipole with the target (σ_{dipole} in Eq. (2.3)). This equation is the simplest manifestation of the fact that the correct degrees of freedom at high energies in QCD, are color dipoles [13].

In the equation (2.1), the rapidity $Y = -\ln x$ and $Y_0 = -\ln x_0$. The ultraviolet cutoff ρ is needed to regularize the integral, but it does not appear in physical quantities. In the large N_c limit (number of colors) $C_F = N_c/2$.

Eq. (2.1) has a very simple meaning: the dipole of size \mathbf{x}_{10} decays in two dipoles of sizes \mathbf{x}_{12} and \mathbf{x}_{02} with the decay probability given by the wave function $|\Psi|^2 = \frac{x_{01}^2}{x_{02}^2 x_{12}^2}$. These two dipoles then interact with the target. The non-linear term takes into account the Glauber corrections for such an interaction.

The linear part of Eq. (2.1) is the BFKL equation[17], which describes the evolution of the multiplicity of the fixed size color dipoles with respect to the energy Y . The nonlinear term corresponds to a dipole splitting into two dipoles and it sums the high twist contributions. Note, that the linear part of Eq. (2.1) (the BFKL equation) also has higher twist contributions and vice versa, the main contribution of the non-linear part is to the leading twist (see Ref. [6] for general arguments and Ref. [18] for explicit calculations).

Eq. (2.1) was suggested in the momentum representation by Gribov, Levin and Ryskin [2] and it was proved in the double log approximation of perturbative QCD by Mueller and Qiu [6], in Wilson Loop Operator Expansion at high energies by Balitsky [10], in color dipole approach [13] to high energy scattering in QCD by Kovchegov [11] and in the effective Lagrangian approach for high parton density QCD by Iancu, Leonidov and McLerran (see Ref. [12] and Refs. [9] for previous efforts). Therefore, it gives a reliable tool for an extrapolation of the parton distribution to the region of low x .

One can see that Eq. (2.1) does not depend explicitly on the target² and all such dependence comes from the initial condition at some initial value x_0 . For a target nucleus it was argued in Ref. [11] that the initial conditions should be taken in the Glauber form:

$$\tilde{N}(\mathbf{x}_{01}, x_0; b) = N_{GM}(\mathbf{x}_{01}, x_0; b), \quad (2.4)$$

with

$$N_{GM}(\mathbf{x}_{01}, x; b) = 1 - \exp \left[-\frac{\alpha_S \pi \mathbf{x}_{01}^2}{2 N_c R^2} x G^{DGLAP}(x, 4/\mathbf{x}_{01}^2) S(\mathbf{b}) \right]. \quad (2.5)$$

The equation (2.5) represents the Glauber-Mueller (GM) formula which accounts for the multiple dipole-target interaction in the eikonal approximation [14, 20, 21]. The function $S(b)$ is a dipole profile function inside the target. The value of x_0 is chosen within the interval

$$\exp\left(-\frac{1}{\alpha_S}\right) \leq x_0 \leq \frac{1}{2mR}, \quad (2.6)$$

²This independence is a direct indication that the equation is correct for all targets (hadron and nuclei) in the regime of high parton density.

where R is the radius of the target. In this region the value of x_0 is small enough to use the low x approximation, but the production of the gluons (color dipoles) is still suppressed as $\alpha_S \ln(1/x) \leq 1$. Therefore, in this region we have the instantaneous exchange of the classical gluon fields. Hence, an incoming color dipole interacts separately with each nucleon in a nucleus (see Mueller and Kovchegov paper in Ref. [8]).

For the hadron, however, we have no proof that Eq. (2.4) is correct. As far as we understand the only criteria in this problem (at the moment) is the correct description of the experimental data. We described almost all available HERA data using Eq. (2.4) [22, 23], and we feel confident using Eq. (2.4) as an initial condition for Eq. (2.1). In our model we use the Gaussian $S(b) = e^{-b^2/R^2}$ form for the profile function of the hadron. The parameter R is a phenomenological input, while the gluon density xG^{DGLAP} is a solution of the DGLAP equation. For x_0 we have Eq. (2.6) for a hadron target as well, but practically we choose $x_0 = 10^{-2}$ which satisfies Eq. (2.6) and for which we much experimental data exists to check our initial conditions.

Solutions to the equation (2.1) were studied in asymptotic limits in Ref. [24]. A first numerical attempt to solve an equation similar to the equation (2.1) was reported in Ref. [25]. However, the solution was only obtained for nuclei, and the main emphasize was put on extremely small values of x . In the following section we report on our approach to find a numerical solution of the equation (2.1) which differs completely from the one adopted in [25], as we use the coordinate representation in which the initial conditions are of a very simple form (see Eq. (2.4)). The second reason for using the coordinate representation is the fact that all physical observables can be expressed in terms of the amplitude for the dipole-target interaction in the coordinate representation (see below for xG).

Unfortunately, equation (2.1) is an approximate one. It sums large $\ln x$ contributions only. The situation can be improved at small distances, as the exact x dependence of the kernel is known as this is the DGLAP kernel. An attempt to obtain the elastic amplitude N based on elements of both the equation (2.1) and DGLAP equation was presented in Ref. [4]. The authors of that paper first solve a generalized DGLAP-BFKL linear equation [26], and then add to the solution a nonlinear perturbation of the form presented in the equation (2.1). This approach actually incorporates the high twist contributions in the standard way, treating them as corrections to the leading one.

We suggest a different approach to the problem. First, all twist contributions should be summed by solving equation (2.1). We denote by \tilde{N} a solution of equation (2.1). Second, we add to the obtained solution a correcting function ΔN , which will account for the DGLAP kernel:

$$N = \tilde{N} + \Delta N. \quad (2.7)$$

Assuming ΔN to be small relatively compared to \tilde{N} , we propose the following linear equation for $\Delta N(r_\perp, x; b) = r_\perp^2 B(2/r_\perp, x; b)$:

$$\begin{aligned} \frac{dB(Q, x; b)}{d(\ln Q^2)} &= \frac{C_F \alpha_S}{\pi} \int_{x/x_0}^1 P_{g \rightarrow g}(z) B(Q, \frac{x}{z}; b) dz - \\ &\frac{2 C_F \alpha_S}{\pi} \int_{x/x_0}^1 \frac{dz}{z} \tilde{N}(2/Q, \frac{x}{z}; b) B(Q, \frac{x}{z}; b) + \frac{Q^2 C_F \alpha_S}{4\pi} \int_{x/x_0}^1 \left(P_{g \rightarrow g}(z) - \frac{2}{z} \right) \tilde{N}(2/Q, \frac{x}{z}; b) dz \end{aligned} \quad (2.8)$$

Here $P_{g \rightarrow g}(z)$ stands for the usual gluon splitting function:

$$P_{g \rightarrow g}(z) = 2 \left[\frac{1-z}{z} + \frac{z}{(1-z)_+} + z(1-z) + \left(\frac{11}{12} - \frac{n_f}{18} \right) \delta(1-z) \right]. \quad (2.9)$$

Equation (2.8) is a linear equation valid in the leading $\ln Q^2$ approximation, with $Q^2 = 4/r_\perp^2$. The last term in the equation represents the correction which is due to the substitution of the BFKL kernel $1/z$ by the correct DGLAP kernel. The first term on the right hand side of the equation (2.8) is the DGLAP evolution for the correcting function ΔN , while the second term is the ‘nonlinear ‘interaction’ of the solutions. The initial condition $\Delta N(r_{\perp 0}, x; b) = N(r_{\perp 0}, x; b) - \tilde{N}(r_{\perp 0}, x; b)$ is a phenomenological input at some initial distance $r_{\perp 0} = 2/Q_0$ to be specified. In the present paper we report on our solution of equation (2.1), while leaving the question of the determination of ΔN to another paper.

3 Numerical solution of the nonlinear equation

In this section we report on the exact numerical solution of the equation (2.1) with the initial condition (2.4). For the transverse hadron size the value $R^2 = 10 \text{ (GeV}^{-2}\text{)}$ is taken, this corresponds to the value which is obtained from ‘soft’ high energy phenomenology [19, 27] and is in agreement with HERA data on J/Ψ photo-production [28]. For $xG^{DGLAP}(x, Q^2)$ we use the GRV’94 parameterization and the leading order solution of the DGLAP evolution equation [29]. The kinematic region where the solution of (2.1) is found, ranges in x from 10^{-2} , where the initial conditions are set, to $x = 10^{-7}$. The maximal distance is taken to be one fermi. The value of the ultraviolet cutoff ρ is $2 \times 10^{-4} \text{ (GeV}^{-1}\text{)}$. The numerical solutions obtained are checked to be independent of this choice. In all previous studies of equation (2.1) the formal dependence on the impact parameter b was omitted. As our first step we too will neglect the b -dependence. Later we will consider the impact parameter dependence.

3.1 Solution without b -dependence.

In this subsection we assume that both sides of the equation (2.1) do not depend on the impact parameter b . In a sense, the assumption formally corresponds to the $b = 0$ case, though the whole approach is based on the dipole picture where the impact parameter is larger than the dipole sizes.

We propose to solve the equation (2.1) by the method of iterations. Equation (2.1) can be rewritten

$$\begin{aligned} \tilde{N}_{i+1}(\mathbf{x}_{01}, Y) \equiv \tilde{N}_{i+1}(\mathbf{x}_{01}, Y; b=0) &= \tilde{N}_i(\mathbf{x}_{01}, Y_0) e^{-\frac{2C_F \alpha_S}{\pi} \ln\left(\frac{x_{01}^2}{\rho^2}\right)(Y-Y_0)} + \frac{C_F \alpha_S}{\pi^2} \times \\ &\int_{Y_0}^Y dy e^{-\frac{2C_F \alpha_S}{\pi} \ln\left(\frac{x_{01}^2}{\rho^2}\right)(Y-y)} \int_\rho d^2 \mathbf{x}_2 \frac{\mathbf{x}_{01}^2}{\mathbf{x}_{02}^2 \mathbf{x}_{12}^2} \left(2 \tilde{N}_i(\mathbf{x}_{02}, y) - \tilde{N}_i(\mathbf{x}_{02}, y) \tilde{N}_i(\mathbf{x}_{12}, y) \right) \end{aligned} \quad (3.10)$$

$x \setminus \text{iter.}$	10	14	18	22	25
10^{-7}	56%	24%	9%	5%	1%
10^{-6}	50%	20%	7%	4%	1%
10^{-5}	34%	10%	3%	1%	1%
10^{-4}	14%	2%	1%	1%	1%
10^{-3}	1%	1%	1%	1%	1%

Table 1: Convergence of the iterations for the x independent zero iteration. The table shows the maximal relative errors in percent.

$x \setminus \text{iter.}$	8	9	10	11	12
10^{-7}	12%	9%	6%	3%	1%
10^{-6}	10%	7%	4%	2%	1%
10^{-5}	6%	4%	3%	1%	1%
10^{-4}	6%	4%	2%	1%	1%
10^{-3}	3%	2%	1%	1%	1%

Table 2: Convergence of the iterations for the GM input for zero iteration. The table shows the maximal relative errors in percent.

We stop the iterations when the relative error between two iterations $|(\tilde{N}_{i+1} - \tilde{N}_i)/\tilde{N}_i| \ll 1$ in the kinematic region of the interest³. Practically, the iteration is stopped when the maximal relative error between last two iterations is smaller than one percent, which is of the same order as our numerical accuracy. As a zero iteration the initial condition (2.4) is taken, which is a x independent function.

Convergence of the solution for the constant value $\alpha_S = 0.25$ is shown in the Fig. (1). As we go to smaller values of x the number of iterations required for the convergence increases. For $x = 10^{-7}$ the solution is obtained after about 25 iterations. The convergence is very slow because the zero iteration taken is far from the true solution. Table (1) presents the maximal relative errors for various number of performed iterations.

In fact, the number of iterations can be dramatically decreased by guessing a better zero iteration. The GM formula (2.5) provides a reasonable choice. This formula happens to be a good approximation to the solution, thus significantly reducing the process of convergence. Taking the GM formula as the zero iteration, the same solution is obtained again after about a dozen iterations. Table (2) shows the iteration convergence.

Equation (2.1) as well as the BFKL equation is derived for a constant strong coupling α_S . Though some attempts were made to introduce a running coupling constant into the BFKL equation it has not yet been done in a self consistent way. However, the use of the running coupling constant in equation (2.1) is justified in the double logarithmic approximation. Motivated by this fact, a solution of equation (2.1) with running α_S is also obtained.

It is interesting to compare the solutions found with two of the widely used saturation models. The first one is the GM formula (2.5). The second one is the Golec-Biernat and Wusthoff (GW)

³ A formal question of the iteration convergence may certainly arise. Namely, when two iterations are sufficiently close it does not formally mean that a limit has been reached and even if that the limit exists at all. As a counterexample one can consider the sum of the series $1/n$, which diverges though every step decreases. We have to stress that we completely ignore this question. Since a solution to the equation exists and its asymptotics are known, we are confident about correct convergence of our procedure.

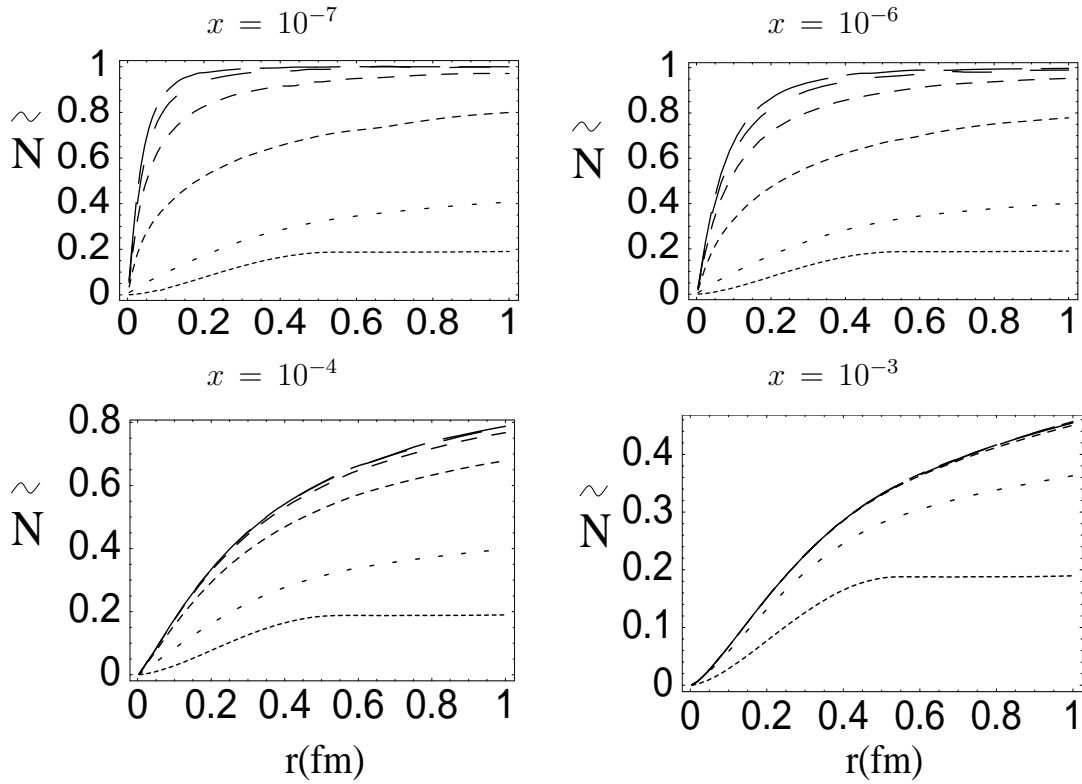


Figure 1: The function \tilde{N} is plotted versus distance (in fermi). The six curves show the convergence of the iterations (from below 1,5,10,14,18,and 25 iterations).

saturation model [30]. In that model the effective dipole cross section $\sigma_{\text{dipole}}^{GW}(x, r_{\perp})$ describing the interaction of the $q\bar{q}$ pair with a nucleon has the form:

$$\sigma_{\text{dipole}}^{GW}(x, r_{\perp}) = \sigma_0 N_{GW}(x, r_{\perp}); \quad N_{GW}(x, r_{\perp}) = [1 - \exp(-r_{\perp}^2/(4R_0^2(x)))];$$

$$R_0(x) = (x/x_0)^{\lambda/2} (\text{GeV}^{-1}); \quad \sigma_0 = 23.03 (\text{mb}); \quad \lambda = 0.288; \quad x_0 = 3.04 \times 10^{-4}.$$

The cross section σ_0 is a dimension-full parameter which properly normalizes the dipole cross section. A natural comparison is between our function \tilde{N} and the dimensionless saturation function N_{GW} of the GW model. The Fig. (2) shows the comparison between our solutions, GM formula, and GW model. It can be seen that the correct numerical solution is obtained between the GM formula and GW model. At large distances $GW \leq \tilde{N} \leq GM$, while at small distances the inverse situation is realized $GM \leq \tilde{N} \leq GW$. We would like to remind the reader that by construction the GM formula is a DGLAP solution at small distances.

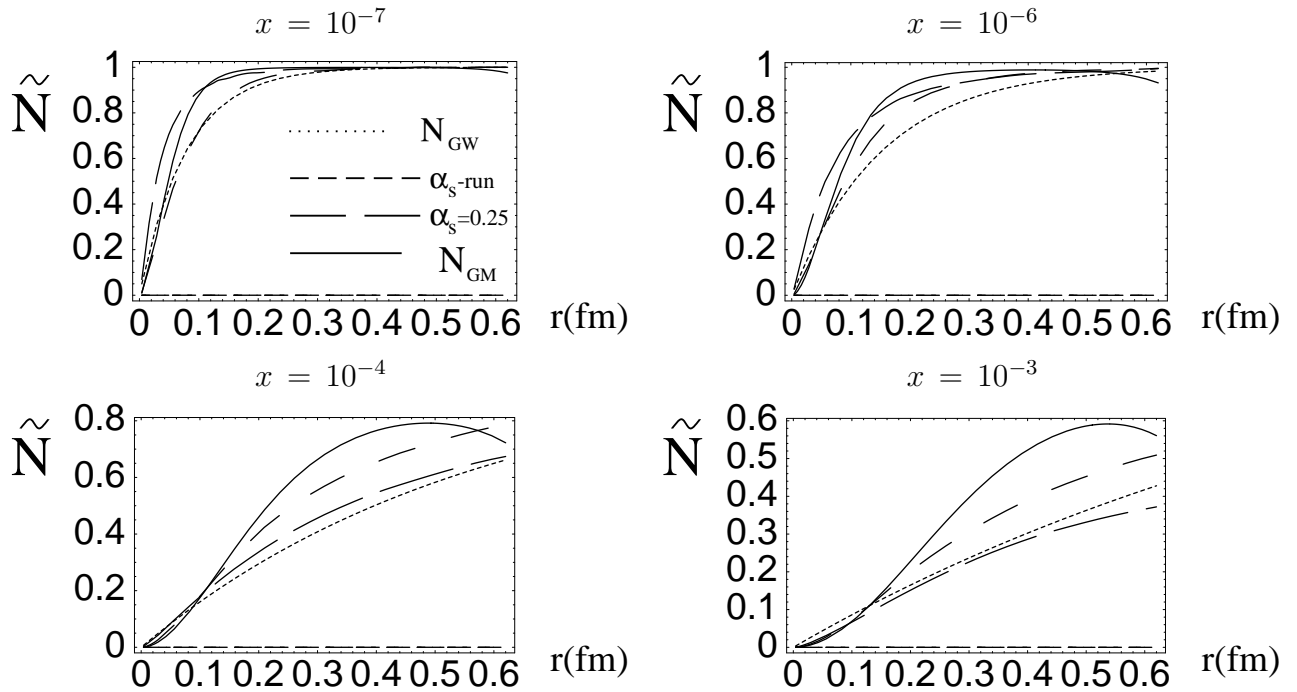


Figure 2: The comparison between the solutions \tilde{N} , Glauber-Mueller formula, and GW model. The four curves correspond to two different solutions $\tilde{N}_{\alpha_s=0.25}$ (large dashes), $\tilde{N}_{\alpha_s\text{-running}}$ (small dashes), N_{GM} (continuous line), and N_{GW} of the GW model (dots).

We would like to add a comment on the behavior of the GM formula at large distances. At fixed x this function has a maximum and then decreases. Such a behavior is certainly unphysical and is just an artifact of using the GRV parameterization which itself possesses a similar behavior.

One of the goals of the present research is to determine the saturation scale $Q_s(x)$. Despite many attempts, no exact mathematical definition of $Q_s(x)$ has so far has been found. However, some reasonable estimates can be obtained from the function \tilde{N} . As can be seen from the figures (1,2)

\tilde{N} behaves in a step like manner as a function of distance: at small distances it tends to zero, while at large distances the saturation value one is approached. For such a step-like kind of function it is natural to define the saturation scale as a position where $\tilde{N} = 1/2$:

$$\tilde{N}(2/Q_s, x) = 1/2. \quad (3.12)$$

The equation (3.12) defines the saturation scale Q_s as a function of x (Fig. (3,a)). The saturation scale of the GW model defined as $1/R_0(x)$ is also displayed in the Fig. (3,a).

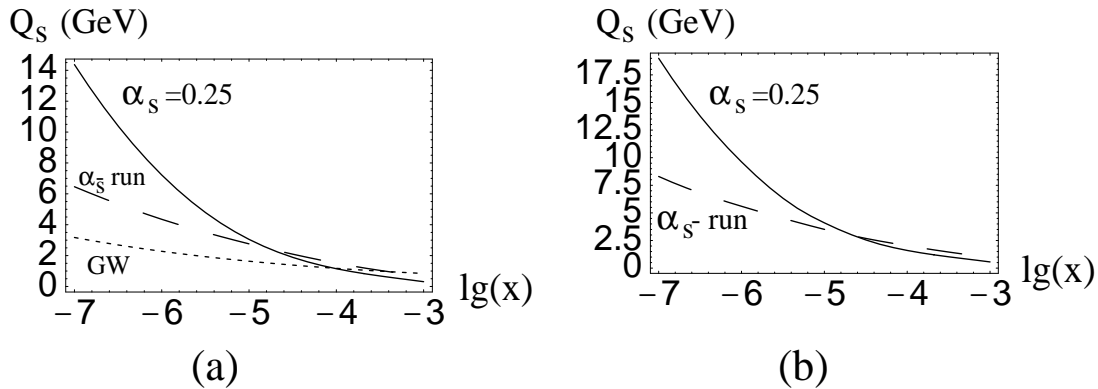


Figure 3: The saturation scale Q_s is plotted as a function $\lg x = \log_{10}(x)$. (a) - the scale obtained from the equation (3.12), the dotted line (GW) corresponds to the saturation scale of the GW model; (b) - the equation (3.19) is used to determine the scale.

We have to comment that the accepted definition of the saturation scale (3.12) is not quite consistent with the estimates obtained from the GM formula. In the latter approach $Q_s(x)$ is deduced from the requirement that the gluon packing factor in a cascade should be equal to unity. For large values of x (10^{-2} - 10^{-4}) the saturation scale thus obtained is somewhat larger than that shown in the Fig. (3,a).

3.2 b -dependence of the solution.

In this subsection we deal with the b -dependence of the equation (2.1). The proposed iteration method can in fact be applied, but in this case the computational time increases dramatically. Instead, we assume that solution of the equation (2.1) preserves the very same b -dependence as introduced by the initial conditions (2.4):

$$\tilde{N}(r_{\perp}, x; b) = (1 - e^{-\kappa(x, r_{\perp}) S(b)}), \quad (3.13)$$

where κ is related to the $b = 0$ solution

$$\kappa(x, r_{\perp}) = -\ln(1 - \tilde{N}(r_{\perp}, x, b = 0)). \quad (3.14)$$

Of course, the assumption requires verification. In order to verify that (3.13) is a solution of (2.1) we should check if it indeed satisfies (2.1). So, we plug \tilde{N} (3.13) into the rhs of (2.1) and

then compare it with $\tilde{N}(lhs(2.1))$. Fig. (4) shows the comparison as a function of the impact parameter b . A good fit is found. The matching becomes worse in the region close to saturation. This happens mainly due to problematic numerical behavior of κ .

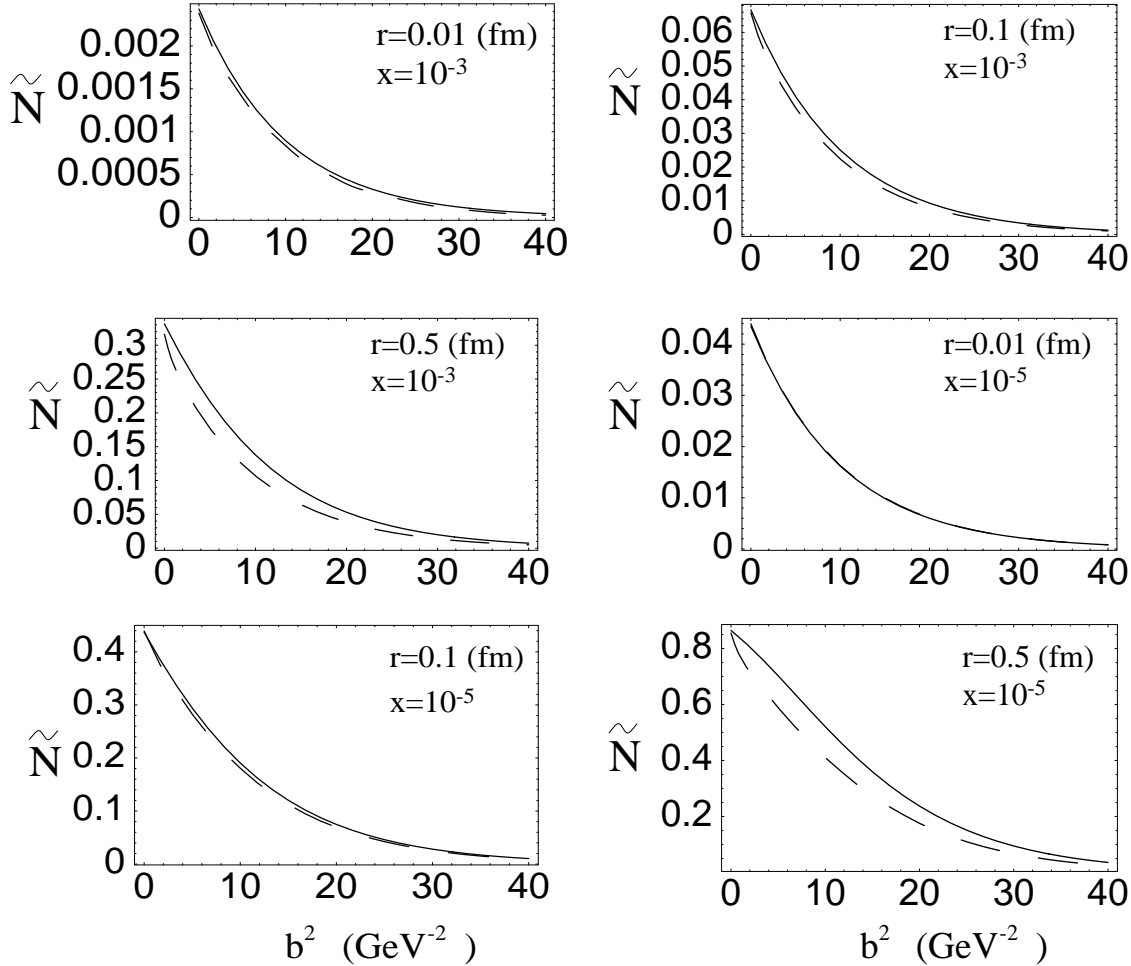


Figure 4: The b -dependence of the solution is compared with the model dependence of the equation (3.13). The graphs are plotted as functions of b^2 for two values of x : $x = 10^{-3}$ and $x = 10^{-5}$. The continuous line is the ansatz (3.13), while the dashed line is $\tilde{N}(lhs(2.1))$.

In order to make an additional estimate of the accuracy of the ansatz (3.13), a solution of the equation (2.1) is obtained for a single value of the impact parameter. The only simplification which is made in this computation is the assumption that the impact parameter b is much larger than the dipole sizes:

$$\mathbf{x}_{01} \ll b; \quad \mathbf{x}_{02} \ll b. \quad (3.15)$$

In this case the b -dependence of the rhs of (2.1) is significantly simplified. This is actually the very same approximation that was used in the previous subsection. Figure (5) presents the comparison of the ansatz (3.13) with numerically computed solution for $b^2 = 10 \text{ GeV}^{-2}$.

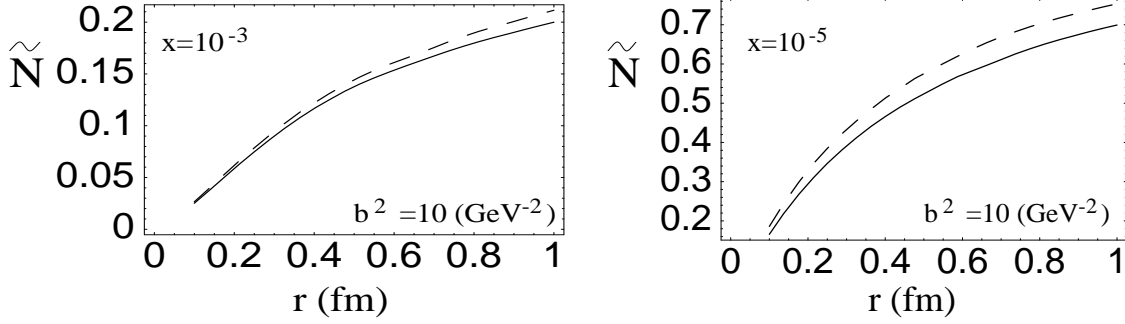


Figure 5: The solution of the eq. (2.1) for $b^2 = 10 \text{ GeV}^{-2}$ is compared with the ansatz dependence of the equation (3.13). The graphs are plotted as functions of distance for two values of x : $x = 10^{-3}$ and $x = 10^{-5}$. The continuous line is the ansatz (3.13), while the dashed line is the exact numeric solution.

The match is quite good at moderate x , though it becomes worse at smaller x . Note, however, from figures (4) and (5) we see that the curve of the ansatz (3.13) is actually squeezed by the two curves it was compared to. This provides an indication of the overall uncertainty of the approximation, which we would roughly estimate not to exceed 10%-20%.

The above procedure cannot be claimed to be a proof of the b -factorization. Moreover, an analytic derivation of the equation (3.13) does not seem to be feasible. However, the solution in the form (3.13) is clearly a satisfactory approximation of the true solution of the equation (2.1).

We can proceed now with the evaluation of the dipole cross section

$$\sigma_{\text{dipole}}(x, r_{\perp}) = 2 \int d^2b \tilde{N}(r_{\perp}, x, b). \quad (3.16)$$

Having assumed (3.13), the dipole cross section has the form

$$\sigma_{\text{dipole}} = 2 \pi R^2 [\ln(\kappa) + E_1(\kappa) + \gamma]. \quad (3.17)$$

In equation (3.17) γ denotes for the Euler constant, while E_1 is the exponential integral function. The expression (3.17) predicts the $\ln \kappa$ growth of the dipole cross section, which is in agreement with the conclusions presented in Ref. [24]. Fig. (6) presents a comparison between σ_{dipole} from (3.17) and the GW model (3.11). From Fig. (6) it can be seen that the ratio $\sigma_{\text{dipole}}/\sigma_{\text{dipole}}^{GW}$ grows with decreasing x . This is in agreement with the logarithmic growth of the dipole cross section σ_{dipole} , while the $\sigma_{\text{dipole}}^{GW}$ is saturated at small values of x .

We define the gluon density xG by using the Mueller formula. It relates the gluon density to the dipole cross section:

$$xG(x, Q^2) = \frac{4}{\pi^3} \int_x^1 \frac{dx'}{x'} \int_{4/Q^2}^{\infty} \frac{dr^2}{r^4} \sigma_{\text{dipole}}(x', r). \quad (3.18)$$

Fig. (7) presents the comparison between the gluon density obtained by (3.18) and the DGLAP input value in the GRV parameterization. At small x DGLAP predicts steep growth of the gluon density (power law). As was expected, the shadowing corrections suppress the growth, and the x growth of the function xG is logarithmic which does not contradict unitarity.

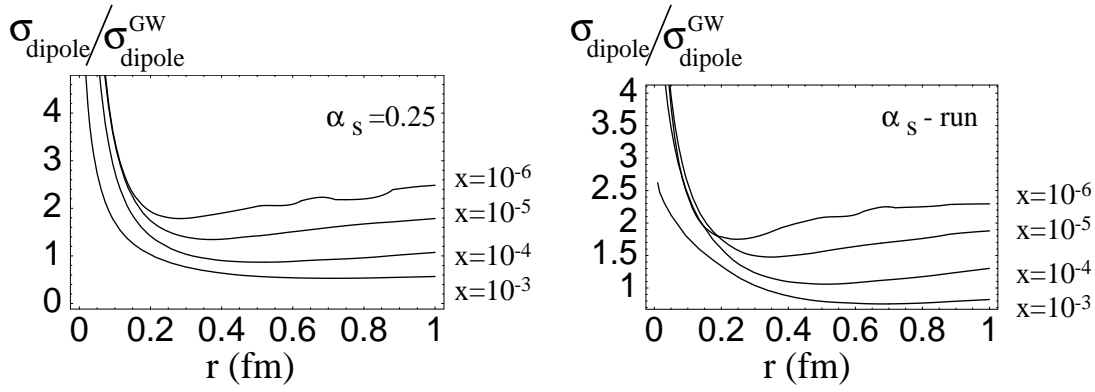


Figure 6: The ratio $\sigma_{\text{dipole}}/\sigma_{\text{dipole}}^{\text{GW}}$ is plotted as a function of distance for different values of x .

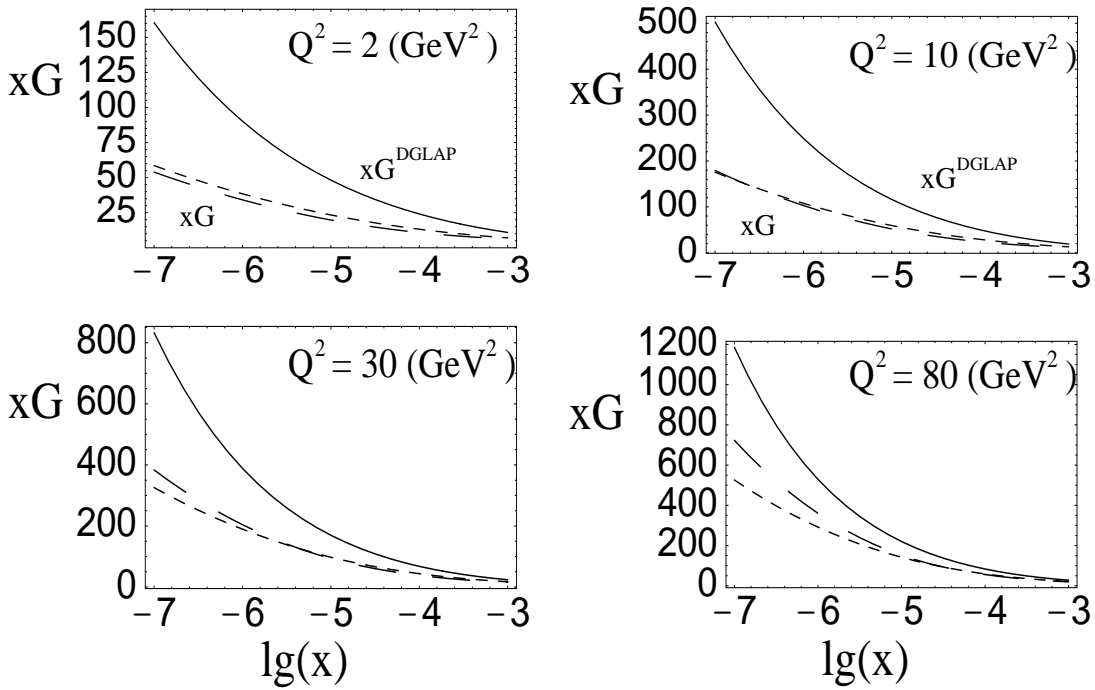


Figure 7: The function xG is plotted versus $\lg(x)$. The small dashes correspond to the solution with the running α_S , while the large dashes are used for the constant $\alpha_S = 0.25$. The continuous line is the GRV parameterization.

The gluon density xG defined as in (3.18) grows with decreasing x . In a sense, this observation contradicts the “super-saturation” of Ref. [25] where the density is predicted to vanish in the large rapidity limit. However, the gluon density definition accepted in Ref. [25] differs from ours, and hence the functions are not compatible.

It is worth making an additional comment about the saturation scale $Q_s(x)$. In the previous subsection we defined it through the equation (3.12). Here we propose an alternative definition similar to the one adopted in the GM formula. Namely:

$$2 \kappa(x, 2/Q_s) = 1. \quad (3.19)$$

The above definition corresponds to $\tilde{N}(2/Q_s, x, b=0) \simeq 0.4$, and it predicts a somewhat larger saturation scale $Q_s(x)$ (Fig. (3,b)) than the equation (3.12). Comparing the four curves of both figures (3,a) and (3,b) an uncertainty in the $Q_s(x)$ determination can be estimated. It is about 30%-40% through a very large range of x , though reaching 100% uncertainty at $x = 10^{-7}$.

4 DGLAP correction - consistency check

In this section we would like to make some comments regarding the consistency of our approach. It was argued previously that it is necessary to add a correction term ΔN to the solution \tilde{N} of the nonlinear equation (2.1) which we found. In turn, the function ΔN is a solution of the evolution equation (2.8).

Consistency of the approach requires the support of ΔN only at moderate x . The function ΔN should give vanishing contributions at very small x . We also expect this function to decrease with Q^2 . In order to check the above conditions some asymptotic estimates can be made without explicitly solving the equation (2.8).

At very small x and large distances the function $\tilde{N} \simeq 1$. For this case equation (2.8) can be rewritten:

$$\frac{dB(Q, x)}{d(\ln Q^2)} = \frac{C_F \alpha_S}{\pi} \int_{x/x_0}^1 \left(P_{g \rightarrow g}(z) - \frac{2}{z} \right) \left(\frac{Q^2}{4} \tilde{N}(2/Q, \frac{x}{z}) + B(Q, \frac{x}{z}) \right) dz. \quad (4.20)$$

The main observation is that the evolution kernel entering the equation (4.20) is actually negative. Hence the function ΔN is a decreasing function of Q .

We illustrate the point in a model where the anomalous dimension has the form [31]

$$\gamma(\omega) = \frac{\alpha_S N_c}{\pi} \left(\frac{1}{\omega} - 1 \right), \quad (4.21)$$

where the anomalous dimension is defined by the Mellin transform of the splitting function $P_{g \rightarrow g}$:

$$\gamma(\omega) = \frac{\alpha_S C_F}{\pi} \int_0^1 dz P_{g \rightarrow g}(z) z^\omega. \quad (4.22)$$

We represent the functions B and \tilde{N} through their inverse Mellin transforms:

$$B(Q, x) = \frac{1}{2\pi i} \int_C d\omega x^{-\omega} B(Q, \omega); \quad \tilde{N}(2/Q, x) = \frac{1}{2\pi i} \int_C d\omega x^{-\omega} \tilde{N}(2/Q, \omega).$$

The equation (4.20) can be now expressed in the following form:

$$\frac{dB(Q, \omega)}{d(\ln Q^2)} = -\frac{\alpha_S N_c}{\pi} \left[\frac{Q^2}{4} \tilde{N}(2/Q, \omega) + B(Q, \omega) \right]. \quad (4.23)$$

The solution of the equation (4.23) is:

$$B(Q, \omega) = (Q^2)^{-\bar{\alpha}_S} \left[-\frac{\bar{\alpha}_S}{4} \int_{Q_0^2}^{Q^2} \tilde{N}(2/Q', \omega) (Q'^2)^{\bar{\alpha}_S} dQ'^2 + C(\omega) \right], \quad (4.24)$$

with $\bar{\alpha}_S = \alpha_S N_c / \pi$. The function $C(\omega)$ should be determined by initial conditions at $Q = Q_0$. At very small x and not too large Q the function $N \simeq 1$ and it is a slowly varying function of Q . Hence, it can be taken outside of the integral in (4.24) and we obtain the solution

$$B(Q, \omega) \simeq -\frac{\bar{\alpha}_S/4}{1 + \bar{\alpha}_S} \tilde{N}(2/Q, \omega) Q^2 + \frac{C(\omega)}{(Q^2)^{\bar{\alpha}_S}}. \quad (4.25)$$

As a result for the correcting function ΔN we have:

$$\Delta N(2/Q, x) \simeq -\frac{\bar{\alpha}_S}{1 + \bar{\alpha}_S} \tilde{N}(2/Q, x) + \frac{4C(x)}{(Q^2)^{1+\bar{\alpha}_S}}. \quad (4.26)$$

Recall that in the large Q^2 limit $r_{\perp}^2 = 4/Q^2$. The solution found in (4.26) is in agreement with assumptions made. The function ΔN decreases at small distances and is of size $O(\alpha_S)$ compared to \tilde{N} . The argument presented above only aimed to prove the self consistency of our approach. However, the complete numerical solution of the equation (2.8) is still valid for phenomenological reasons. The initial conditions for the function ΔN should be chosen to fit the experimental data.

5 Numerical solution of the BFKL equation

In this section we report on the numerical solution of the BFKL equation, which is the linear part of the equation (2.1):

$$N_{\text{BFKL}}(\mathbf{x}_{01}, Y) = N_{\text{BFKL}}(\mathbf{x}_{01}, Y_0) \exp \left[-\frac{2C_F \alpha_S}{\pi} \ln \left(\frac{\mathbf{x}_{01}^2}{\rho^2} \right) (Y - Y_0) \right] + \quad (5.27)$$

$$\frac{C_F \alpha_S}{\pi^2} \times \int_{Y_0}^Y dy \exp \left[-\frac{2C_F \alpha_S}{\pi} \ln \left(\frac{\mathbf{x}_{01}^2}{\rho^2} \right) (Y - y) \right] \int_{\rho} d^2 \mathbf{x}_2 \frac{\mathbf{x}_{01}^2}{\mathbf{x}_{02}^2 \mathbf{x}_{12}^2} 2 N_{\text{BFKL}}(\mathbf{x}_{02}, y).$$

We restrict our analysis to $b = 0$ case only. The initial conditions are assumed to be proportional to the gluon density at $x_0 = 10^{-2}$:

$$N_{\text{BFKL}}(\mathbf{x}_{01}, x_0) = \frac{\alpha_S \pi \mathbf{x}_{01}^2}{6R^2} xG(x_0, 4/\mathbf{x}_{01}^2). \quad (5.28)$$

In order to obtain a solution of the equation (5.27) the same method of iterations is applied. However, for this case the convergence of the iterations is extremely slow. Dozens of iterations are required in order to get a final result. Fig. (8) presents solutions of the BFKL equation for $\alpha_S = 0.25$ and for running α_S compared with the solutions of the equation (2.1) as well as of the DGLAP equation.

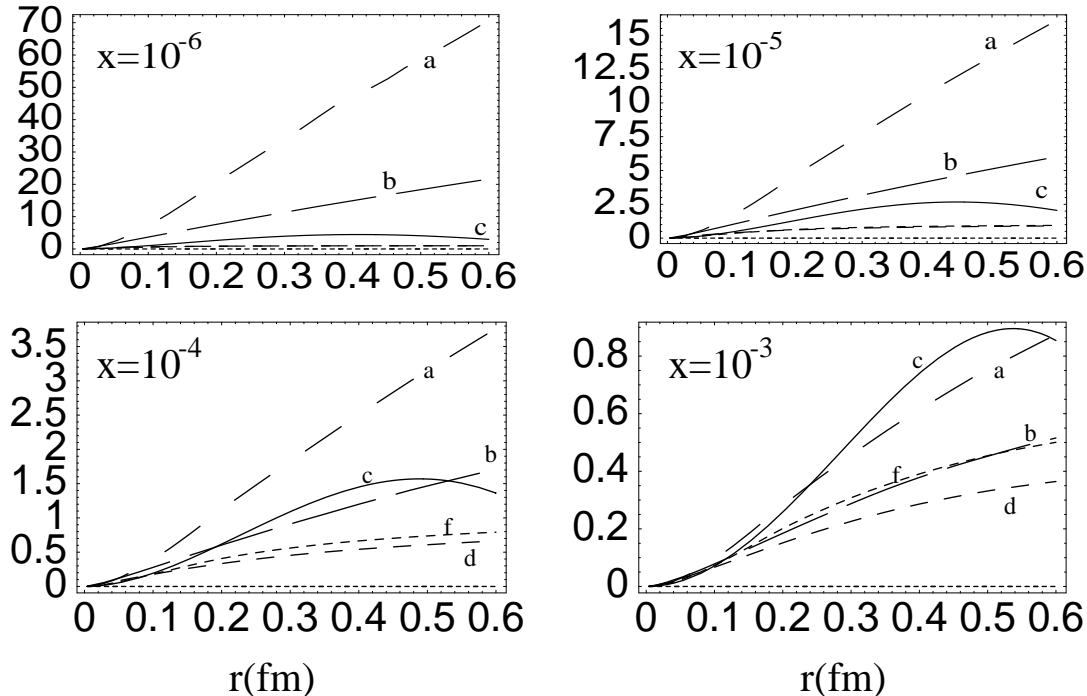


Figure 8: The function N_{BFKL} is plotted together with the solution of the equation (2.1) and the DGLAP equation. *a* - N_{BFKL} for running α_S ; *b* - N_{BFKL} for $\alpha_S = 0.25$; *c* - DGLAP solution in GRV parameterization; *d* - \tilde{N} for $\alpha_S = 0.25$; *f* - \tilde{N} for running α_S .

It is seen from the Fig. (8) that the BFKL equation predicts a very steep growth of the cross section as x decreases. The function N_{BFKL} rapidly diverges from the solutions of the equation (2.1) and of the DGLAP equation. This numerical observation is in fair agreement with previous theoretical considerations about the dynamics of the BFKL equation. The solution of the BFKL equation touches the unitarity bound.

However, the results of BFKL dynamics is unlikely ever to be seen. The nonlinear effects accounted for in the equation (2.1) set in at very small distances thus suppressing the BFKL divergence.

6 Summary

In the present work we suggested a new approach to DIS based on first summing all twist contributions in the leading $\ln x$ approximation. Then, we wrote down a linear evolution equation

for the correcting function which incorporates the correct DGLAP kernel in the leading $\ln Q^2$ approximation.

The method of iterations was successfully applied to the solution of the nonlinear integral equation (2.1). A key observation is the nonlinearity of the equation, and that a good choice for the zero iteration, insures a rapid convergence.

The BFKL equation is solved numerically. Its solution blows up for low values of x , and this is the origin for the possible violation of unitarity. However, the nonlinear effects suppress the growth of the cross section. These effects set in at such small distances that we do not actually ever expect to see the BFKL dynamics.

The nonlinear BFKL-type equation (2.1) is solved numerically. The solution predicts a saturation of the function \tilde{N} at large distances. The dipole cross section obtained is not saturated as a function of x . Due to b integration it grows logarithmically with decrease of x . Fig. (6) shows that the solution to the non-linear evolution equation generates a dipole cross section which is quite different from the predictions of the Golec-Biernat and Wusthoff model [30]. This model is widely used for estimating saturation effects at HERA, and our calculations demonstrate that we should be very careful with the conclusions based on such estimates especially at lower x .

We demonstrated that the solution to the non-linear equation is quite different from the models that have been used for estimates of the saturation effects [22, 30] (see Fig. (2)). However, all these models can be used as a first iteration of the non-linear equation which leads to faster convergence of the numerical procedure.

We found that the non-linear effects are very important for the extrapolations of improved knowledge on the parton distributions to higher energies such as the THERA and LHC energies. Fig. (7) shows that damping due to non-linear effects leads to suppression of a factor of $2 \div 3$ in comparison with the linear DGLAP evolution.

The solution found for the nonlinear equation was used to estimate the saturation scale $Q_s(x)$. In spite of considerable uncertainty in the value of the saturation scale we predict that it grows with decreasing x starting from about 1(GeV) at $x = 10^{-3}$ and reaching around 10(GeV) at $x = 10^{-7}$, in accordance with the theoretical expectations [2, 6, 7, 8].

We proved that the correcting function ΔN is concentrated at the moderate values of x . This fact demonstrates the self-consistency of our approach, as ΔN cannot be large and can be treated using the linear DGLAP-type of equations. The full phenomenological study of the value of ΔN and its x and Q^2 dependence will be published elsewhere.

We hope that our approach will be useful for the extrapolation of the HERA parton distributions to higher energies (lower x). Of course much further work will be required before this area of QCD is fully understood.

Acknowledgements: The authors are very much indebted to our coauthors and friends with whom we discussed our approach on a everyday basis Ian Balitsky, Jochen Bartels, Krystoff Golec Biernat, Larry McLerran, Dima Kharzeev, Yuri Kovchegov and Al Mueller for their help and fruitful discussions on the subject. E.G., E. L. thank BNL Nuclear Theory Group and DESY Theory group for their hospitality and creative atmosphere during several stages of this work.

This research was supported in part by the BSF grant # 9800276, by the GIF grant # I-620-22.14/1999 and by Israeli Science Foundation, founded by the Israeli Academy of Science and Humanities.

References

- [1] V. N. Gribov and L. N. Lipatov, *Sov. J. Nucl. Phys* **15** (1972) 438; G. Altarelli and G. Parisi, *Nucl. Phys.* **B 126** (1977) 298; Yu. I. Dokshitser, *Sov. Phys. JETP* **46** (1977) 641.
- [2] L. V. Gribov, E. M. Levin, and M. G. Ryskin, *Nucl. Phys.* **B 188** (1981) 555.
- [3] J. Bartels, *Phys. Lett.* **B 298** (1993) 204, *Z. Phys.* **C 60** (1993) 471;
E.M. Levin, M.G. Ryskin, and A.G. Shuvaev, *Nucl. Phys.* **B 387** (1992) 589.
- [4] M. A. Kimber, J. Kwiecinski, and A. D. Martin, IPPP-01/01, DCPT/01/02, hep-ph/0101099.
- [5] M. Klein, “*THERA-electron proton scattering at $\sqrt{s} \approx 1 TeV$ ”, talk given at DIS’2000, Liverpool, April 25 - 30, 2000.*
- [6] A. H. Mueller and J. Qiu, *Nucl. Phys.* **B 268** (1986) 427.
- [7] L. McLerran and R. Venugopalan, *Phys. Rev.* **D 49** (1994) 2233, 3352; **D 50** (1994) 2225, **D 53** (1996) 458, **D 59** (1999) 094002.
- [8] E. Levin and M.G. Ryskin, *Phys. Rep.* **189** (1990) 267;
J. C. Collins and J. Kwiecinski, *Nucl. Phys.* **B 335** (1990) 89;
J. Bartels, J. Blumlein, and G. Shuler, *Z. Phys.* **C 50** (1991) 91;
E. Laenen and E. Levin, *Ann. Rev. Nucl. Part. Sci.* **44** (1994) 199 and references therein;
A. L. Ayala, M. B. Gay Ducati, and E. M. Levin, *Nucl. Phys.* **B 493** (1997) 305, **B 510** (1990) 355;
Yu. Kovchegov, *Phys. Rev.* **D 54** (1996) 5463, **D 55** (1997) 5445, **D 61** (2000) 074018;
A. H. Mueller, *Nucl. Phys.* **B 572** (2000) 227, **B 558** (1999) 285;
Yu. V. Kovchegov, A. H. Mueller, *Nucl. Phys.* **B 529** (1998) 451.
- [9] J. Jalilian-Marian, A. Kovner, L. McLerran, and H. Weigert, *Phys. Rev.* **D 55** (1997) 5414;
J. Jalil H. Weigert, NORDITA-2000-34-HE, hep-ph/0004044; J. Jalilian-Marian, A. Kovner, and H. Weigert, *Phys. Rev.* **D 59** (1999) 014015; J. Jalilian-Marian, A. Kovner, A. Leonidov, and H. Weigert, *Phys. Rev.* **D 59** (1999) 034007, Erratum-ibid. *Phys. Rev.* **D 59** (1999) 099903; A. Kovner, J. Guilherme Milhano, and H. Weigert, OUTP-00-10P, NORDITA-2000-14-HE, hep-ph/0004014; H. Weigert, NORDITA-2000-34-HE, hep-ph/0004044.
- [10] Ia. Balitsky, *Nucl.Phys.* **B 463** (1996) 99.
- [11] Yu. Kovchegov, *Phys. Rev.* **D 60** (2000) 034008.

- [12] E. Iancu, A. Leonidov, and L. McLerran, “Nonlinear Gluon Evolution in the Color Glass Condensate”, BNL-NT-00/24, hep-ph/0011241.
- [13] A. H. Mueller, *Nucl. Phys.* **B 415** (1994) 373.
- [14] A. H. Mueller, *Nucl. Phys.* **B 335** (1990) 115.
- [15] N. N. Nikolaev and B. G. Zakharov, *Z. Phys.* **C 49** (1991) 607; E. M. Levin, A. D. Martin, M. G. Ryskin, and T. Teubner, *Z. Phys.* **C 74** (1997) 671.
- [16] V. N. Gribov, *Sov. Phys. JETP* **30** (1970) 709.
- [17] E. A. Kuraev, L. N. Lipatov, and F. S. Fadin, *Sov. Phys. JETP* **45** (1977) 199; Ya. Ya. Balitsky and L. N. Lipatov, *Sov. J. Nucl. Phys.* **28** (1978) 22 .
- [18] J. Bartels, K. Golec-Biernat and K. Peters, *Eur. Phys. J.* **C17** (2000) 121, hep-ph/0003042; E. Gotsman, E. Levin, L. McLerran, and K. Tuchin, *Nucl. Phys.* **B**, in press, hep-ph/0008280.
- [19] A. Donnachie and P. V. Landshoff, *Nucl. Phys.* **B 244** (1984) 322, **B 267** (1986) 690; *Phys. Lett.* **B 296** (1992) 227; *Z. Phys.* **C 61** (1994) 139.
- [20] A. Zamolodchikov, B. Kopeliovich, and L. Lapidus, *JETP Lett.* **33** (1981) 595.
- [21] E. M. Levin and M. G. Ryskin, *Sov. J. Nucl. Phys.* **45** (1987) 150.
- [22] E. Gotsman, E. Levin, and U. Maor, *Nucl. Phys.* **B 464** (1996) 251; **B 493** (1997) 354; E. Gotsman, E. Levin, M. Lublinsky, U. Maor, E. Naftali, and K. Tuchin, hep-ph/0010198, DESY-00-149.
- [23] E. Gotsman, E. Levin, M. Lublinsky, U. Maor, and K. Tuchin, hep-ph/0007261.
- [24] Yu. Kovchegov, *Phys. Rev.* **D 61** (2000) 074018; E. Levin and K. Tuchin, *Nucl. Phys.* **B 573** (2000) 833; hep-ph/0012167.
- [25] M. Braun, *Eur. Phys. J.* **C 16** (2000) 337; hep-ph/0101070.
- [26] J Kwiecinski, A. D. Martin, and A. M. Stasto, *Phys. Rev.* **D 56** (1997) 3991.
- [27] E. Gotsman, E. Levin, and U. Maor, *Phys. Lett.* **B 452** (1999) 287; *Phys. Rev.* **D 49** (1994) 4321; *Phys. Lett.* **B 304** (1993) 199, *Z. Phys.* **C 57** (1993) 672.
- [28] H1 Collaboration: S. Aid et al., *Nucl. Phys.* **B 472** (1996) 3; ZEUS Collaboration: M. Derrick et al., *Phys. Lett.* **B 350** (1996) 120.
- [29] M. Gluck, E. Reya, and A. Vogt, *Eur. Phys. J.* **C 5** (1998) 461.
- [30] K. Golec-Biernat and M. Wüsthoff, *Phys. Rev.* **D 59** (1999) 014017.
- [31] R. K. Ellis, Z. Kunszt, and E. M. Levin, *Nucl. Phys.* **B 420** (1994) 517.